Journal of Nuclear Materials 389 (2009) 233–238

Contents lists available at ScienceDirect

Journal of Nuclear Materials

journal homepage: www.elsevier.com/locate/jnucmat

He ion irradiation damage in Fe/W nanolayer films

Nan Li [a], E.G. Fu [a], H. Wang [b], J.J. Carter [c], L. Shao [c], S.A. Maloy [d], A. Misra [e], X. Zhang [a,*]

[a] Department of Mechanical Engineering, Materials Science and Engineering Program, Texas A&M University, College Station, TX 77843-3123, USA
[b] Department of Electrical and Computer Engineering, Texas A&M University, College Station, TX 77843-3128, USA
[c] Department of Nuclear Engineering, Texas A&M University, College Station, TX 77843-3133, USA
[d] Materials Science and Technology Division, Los Alamos National Laboratory, Los Alamos, NM 87545, USA
[e] Materials Physics and Application Division, Los Alamos National Laboratory, Los Alamos, NM 87545, USA

A B S T R A C T

We report on the evolution of microstructure and mechanical properties of Fe/W multilayers subjected to helium ion irradiations. Sputtered Fe/W multilayers with individual layer thickness, varying from 1 to 200 nm, were subjected to He^+ ion irradiation with a peak displacement per atom value of 6 at ambient temperatures. Helium bubbles, 1–2 nm in diameter, were observed in Fe and W, and more so along layer interfaces. The magnitude of hardness variation after radiation depends on the individual layer thickness. Radiation hardening is observed in specimens with individual layer thickness of $\geqslant 5$ nm. At smaller layer thickness, the hardness barely changes. Analysis indicates that radiation hardening may originate mainly from dislocation loops and partially from He bubbles.

© 2009 Elsevier B.V. All rights reserved.

1. Introduction

High energy helium (He) ion irradiation of metals generates a large number of defects, including vacancies and interstitials, He bubbles and dislocation loops [1–3]. Radiation typically degrades the mechanical properties of metals, most notably an increase in yield strength, and significant loss of ductility (embrittlement) [4]. Radiation induced defects in metals are of great interest, because these defects determine the performance of irradiated materials in nuclear reactor environment. He bubbles and dislocation loops are two major types of radiation induced defects. The solid solubility of He in metals is very low [5]. Thus, at relatively low concentrations of implanted He, it is easy to form He-vacancy clusters, which act as the nucleus for He bubble formation [6]. Once nucleated, in order to maintain a mechanical equilibrium between their internal pressure and the sintering stress, $2\gamma/r$, where γ is the surface energy and r is the bubble radius, the bubbles grow by absorbing He atoms and radiation induced vacancies [7]. High energy He ion bombardment of metals also produces recoil interstitial metal atoms that collapse into prismatic dislocation loops. Different types of defects have different obstacle strengths for glide dislocations. In general, voids and large precipitates act like Orowan barriers and have large barrier strengths; small bubbles, small clusters and network dislocations have relatively small barrier strengths. Lucas reviewed the mechanical properties of austenitic stainless steels [8], and found that at low temperature (~373 K), radiation hardening was dominated by Frank loops at low dose, and by the network dislocations at higher dose. At higher temperature, ~673 K, voids and bubbles begin to contribute to hardening, especially at high dose. Other studies on irradiated 316LN stainless steel show, at approximately 1 at.% He concentration, dislocations and loops can be pinned by He bubbles in the lattice [9].

Recent studies have shown that interfaces in composite materials can act as sinks for radiation induced defects, promote recombination of unlike point defects, and result in enhanced radiation tolerance as compared to conventional single-phase bulk metals [10–12]. For instance, He ion irradiated Cu/Nb multilayer films with a few nm layer thickness seem to suppress the burst of He bubbles after annealing [10]. In this study, we chose Fe/W multilayers for radiation damage studies. Compared to Cu, Fe and W have relatively high melting points, and more open crystal structure, bcc vs. fcc. Molecular dynamics simulations suggest that the characteristics of interface could be a major factor in determining the accumulation of radiation damage in composite materials [13]. The lattice parameter difference between Fe and W is rather large (~10%), and so the Fe/W interface is incoherent [14]. Such incoherent interface could enhance the capability of defect storage. The study will also allow a comparison of incoherent bcc/bcc Fe/W interface with incoherent fcc/bcc Cu/Nb interface.

2. Experimental procedures

Fe/W multilayers were deposited by magnetron sputtering at room temperature on SiO_2 substrates. The vacuum chamber was evacuated to a base pressure less than 5×10^{-8} torr prior to deposition. The constituents within the multilayers have equal layer thickness, varying from 1 to 200 nm. The total film thickness was

* Corresponding author. Tel.: +1 979 845 2143; fax: +1 979 845 3081.
E-mail address: zhangx@tamu.edu (X. Zhang).

0022-3115/$ - see front matter © 2009 Elsevier B.V. All rights reserved.
doi:10.1016/j.jnucmat.2009.02.007

about 2 μm. After deposition, films were implanted at room temperature with 100 keV He^+ ions to a fluence of $6 \times 10^{16}/cm^2$. The beam current is around 6 microamps and the temperature of the stage is around 50 °C during implantation. Transmission electron microscopy (TEM) was performed on a JOEL 2010 microscope operated at 200 kV. Selected area diffraction (SAD) studies were performed with an aperture of 100 nm in diameter. X-ray diffraction (XRD) experiments were performed on Bruker D8-Focus Bragg-Brentano X-ray diffractometer. The hardness and modulus of multilayers before and after irradiation were measured at room temperature by a Fischerscope HM2000XYp instrument with Vickers indenter at an indentation depth down to 250 nm. The instrumented nanoindentation experiment is depth controlled with a typical load of 12–16 mN to achieve an indentation depth of 250 nm. A minimum of nine indents were performed at the same depth on each specimen to get an average hardness value.

3. Results

3.1. Microstructural evolution of irradiated Fe/W multilayers

Distinct Fe (1 1 0) and W (1 1 0) peaks are observed in XRD patterns of Fe/W 50 nm and Fe/W 5 nm multilayers as shown in Fig. 1. Fe/W 5 nm multilayer appears to have stronger Fe (1 1 0) and W (1 1 0) texture than multilayers with greater individual layer thickness. In most cases, after ion irradiation, the peak intensity of Fe and W (1 1 0) drops accompanied with a peak shift to lower angle.

Cross-sectional TEM (XTEM) images reveal radiation induced defects. Fig. 2 shows the microstructure of as-deposited Fe/W 50 nm multilayer film. Both constituents have polycrystalline structure with grains sizes of similar magnitude to that of individual layer thickness, confirmed by inserted SAD pattern. The multilayer films have weak Fe and W {1 1 0} fiber texture perpendicular to the layer interface. The interface between Fe and W is chemically abrupt.

Fig. 3(a–c) shows underfocused bright-field TEM images of ion irradiated Fe/W 50 nm specimens. Fig. 3(a) is taken close to the surface of the film. Very few He bubbles are observed in this region. Fig. 3(b) is taken from the region in which the He concentration is predicted to be the highest by SRIM simulation (as shown by depth dependent He concentration profile in Fig. 4). A very high He bubble density is observed in this region. The diameter of the He bubbles in Fe is ~1.5 nm, slightly greater than that in W. Furthermore the diameter of He bubbles seems to be larger when the bubbles are located along layer interface compared to those inside the layers. 'Black dots' observed from TEM micrographs in the underfocus

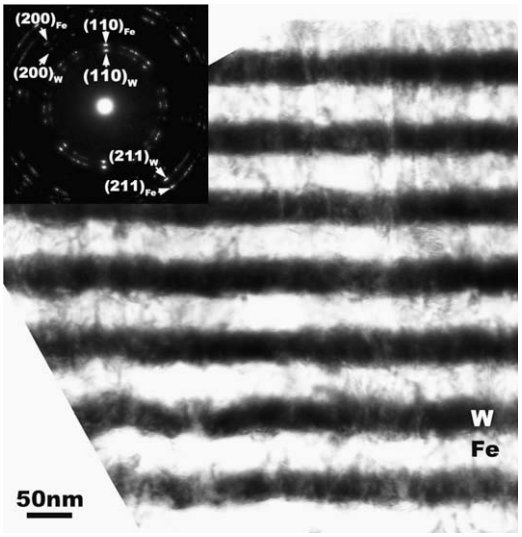

Fig. 2. Cross-sectional TEM (XTEM) image of as-deposited Fe/W 50 nm nanolayer shows clear and unmixed Fe and W layer interface with weak texture.

conditions could be point defect clusters and Frank dislocation loops. At ~600 nm underneath the film surface, Fe and W layers and Fe/W interfaces are essentially intact with no signs of He bubbles, as shown in Fig. 3(c).

SRIM [15] calculation of He ion irradiation has been performed on Fe/W multilayers with a nominal layer thickness of 50 nm. Fig. 4 shows the variation of He concentration versus implantation depth, together with the variation of lattice spacing of Fe (1 1 0) and W (1 1 0), which has been examined from XTEM studies. The simulation predicts that peak He concentration occurs at approximately 300 nm underneath the film surface, with a peak displacement per atom (DPA) of ~6. Measurements of Fe (1 1 0) and W (1 1 0) interplanar spacing from (SAD) patterns were performed with an aperture size of 100 nm in diameter. It can be seen that inter-atomic spacing of Fe (1 1 0) increases rapidly and quickly reaches a plateau at 300 nm, and remains largely distorted up to 500 nm in depth. Whereas lattice distortion in W (1 1 0) seems to take off at a bit deeper level and reaches a peak value at ~500 nm. Lattice expansion maxima of approximately 3% were observed in the peak damage region. Lattice expansions, 1–2%, are also observed (not shown here) from Fe and W (2 0 0) and (2 1 1) diffractions.

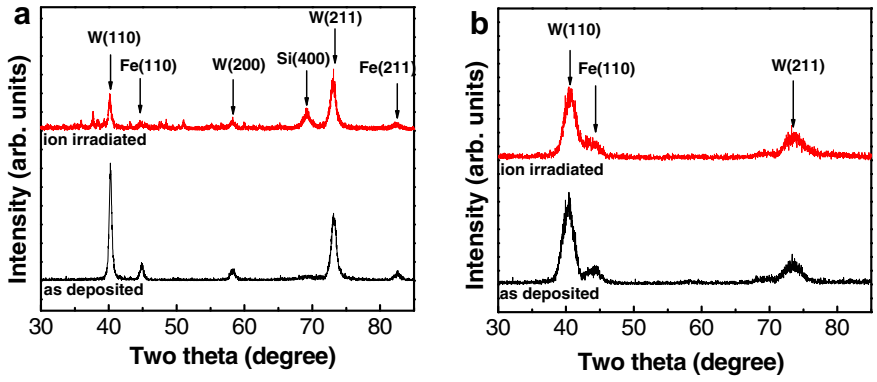

Fig. 1. X-ray diffraction patterns of (a) Fe/W 50 nm multilayers, and (b) Fe/W 5 nm multilayers before and after He ion irradiations. Radiation induces reduction of peak intensity and a shift of peak position to lower angles.

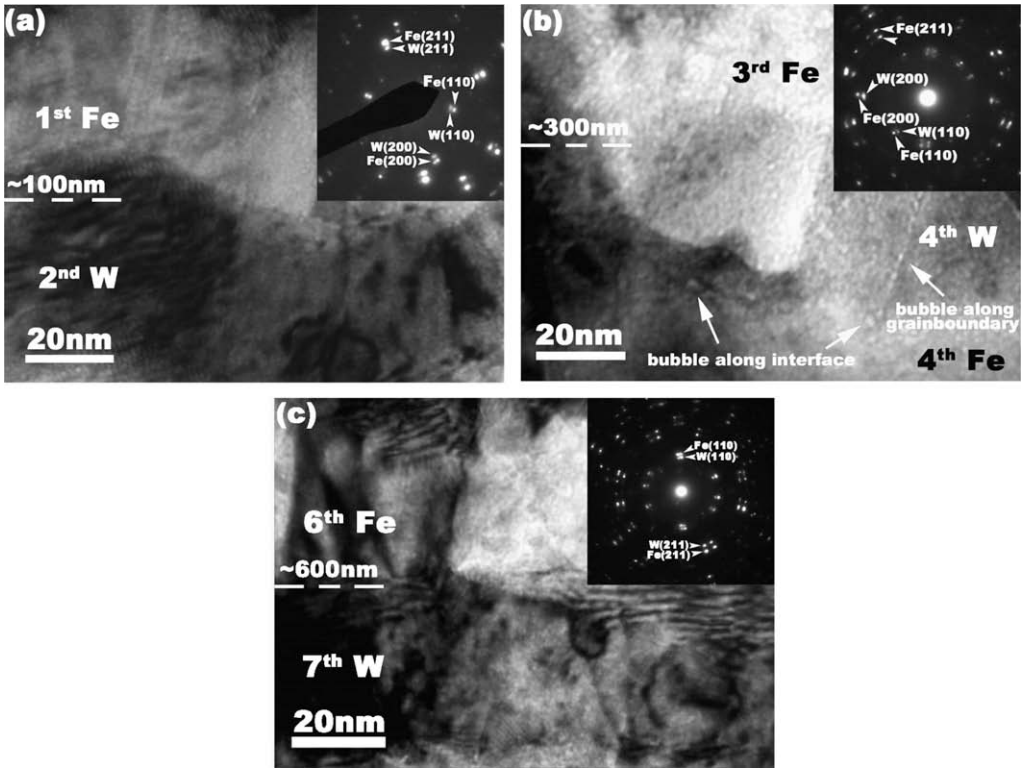

Fig. 3. XTEM image of Fe/W 50 nm nanolayers after ion irradiation. (a) In surface region, moderate amount of He bubbles was observed in Fe and W. (b) In a region of 300 nm underneath film surface, He bubble concentration increases dramatically, and He bubbles align along grain boundary and layer interfaces. (c) In the region of 600 nm underneath film surface, away from radiation damage zone, multilayer films are essentially intact with clear Fe/W interfaces.

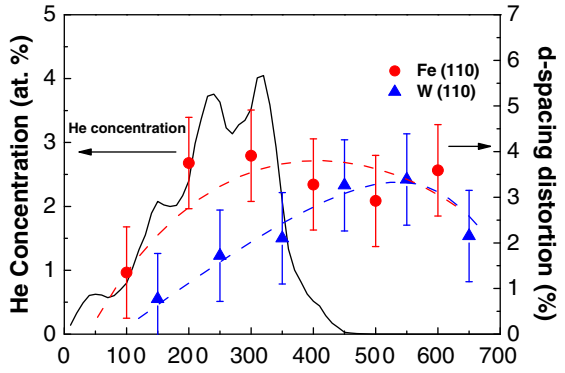

Fig. 4. SRIM calculations that simulate the variation of He concentration versus radiation depth for He ions, 100 keV/6 × 10^{16}/cm^2, same as the experimental condition. Variations of lattice spacing for Fe (110) and W (110) examined by detailed XTEM studies are also shown.

Similar XTEM studies were carried out on ion irradiated Fe/W 1 nm multilayer film. Up to approximately 75 nm below the surface, as shown in Fig. 5(a), a discrete layer structure is not resolved and He bubbles were not detected. Fig. 5(b) shows the microstructure of films, approximately 340 nm below the surface, a region predicted to be heavily damaged based on SRIM simulations. A large number of He bubbles were observed in Fig. 5(b), without clear resolution of layer interfaces. The average He bubble size is ~1–2 nm in diameter. Fig. 5(c), taken at about 420 nm underneath the film surface, shows a reduction of He bubble concentration. The retention of layer structure at the bottom of the region indicates diminishing radiation damage. Radiation damage continues to decrease in deeper regions. At a depth of ~1200 nm underneath the film surface, the microstructure is essentially identical to that of the as-deposited specimens, i.e., the layer structure is clearly distinguishable without signs of radiation damage, as illustrated in Fig. 5(d).

3.2. Mechanical properties

The hardness of as-deposited and ion irradiated Fe/W multilayer films are compared in Fig. 6(a) as a function of $h^{-1/2}$, where h is the thickness of individual layers. For as-deposited multilayers, when h is 50 nm or greater, the hardness of multilayers scales approximately linearly with $h^{-1/2}$, following a Hall–Petch relationship:

$$H = H_0 + kh^{-\frac{1}{2}}, \tag{1}$$

where H is the hardness of the thin film, H_0 is film hardness at infinitely large layer thickness and k is the Hall–Petch slope, measuring the relative hardening contribution from layer interfaces. A linear fit to the experimental data is indicated by a solid line in the plot, yields H_0 = 4.7 GPa and k = 42.9 GPa nm$^{0.5}$. As the individual layer thickness decreases even further, the film hardness increases nonlinearly, and reaches a peak hardness of 35.4 GPa at h = 1 nm. Radiation induces hardening in almost all multilayer films. When layer thickness is larger than 20 nm, the Hall–Petch relationship is also observed, as indicated by a dash line in the plot. The Hall–Petch slope of irradiated multilayers is 35.4 GPa nm$^{0.5}$, smaller than that of as-deposited multilayer system. To compare the magnitude of radiation hardening, ΔH, a plot of ΔH vs. $1/h^{1/2}$ is shown in Fig. 6(b). Specifically, after He ion irradiation, the hardness of multilayers increases by 1.5–2 GPa when $h \geqslant 5$ nm. Radiation hardening is less significant when h = 2.5 nm, and hardness barely changes when h = 1 nm.

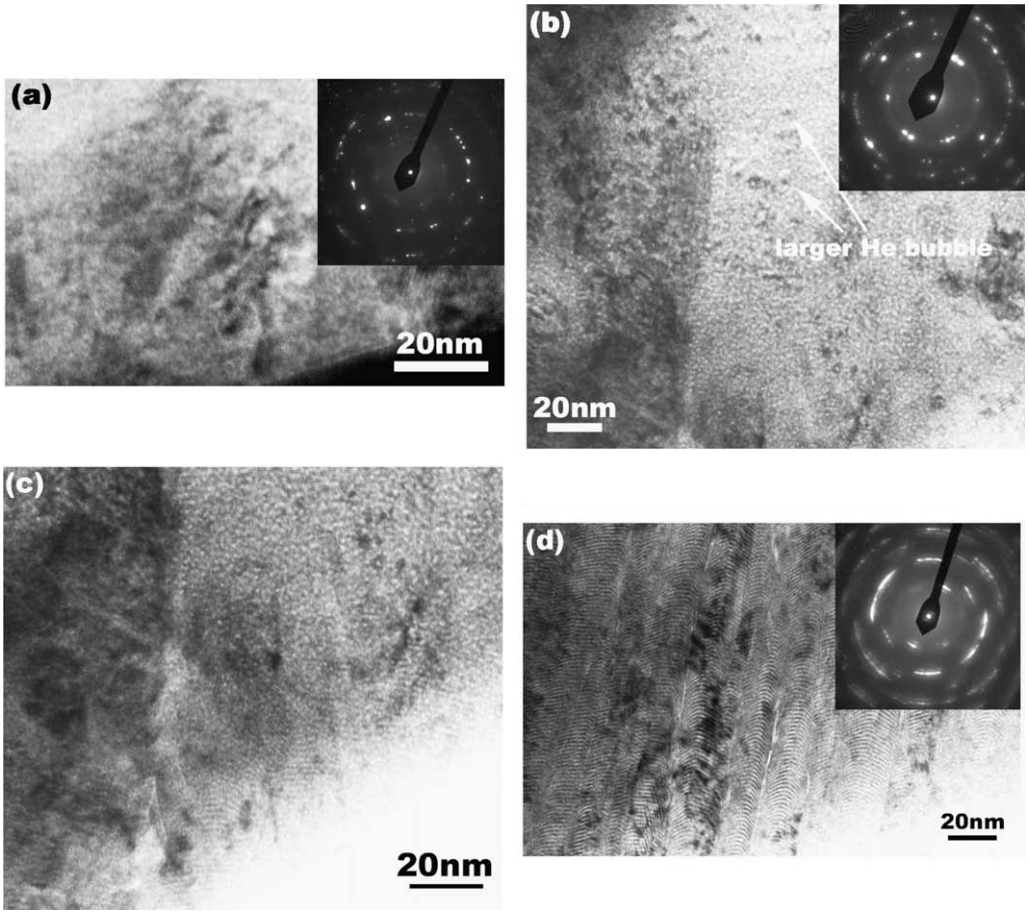

Fig. 5. XTEM images of Fe/W 1 nm multilayer film after He ion irradiation. (a) Microstructure in surface region, ~75 nm underneath the film surface, has little He bubbles and no clear sign of layer interfaces. (b) In heavily irradiated region, ~340 nm below film surface, He bubble density reaches a peak value. Fe and W interface can not be detected. (c) In a region of ~420 nm underneath film surface, the density of He bubbles decreases, and at the bottom of this region, layer structure is distinguishable. (d) In an essentially unirradiated region of ~1200 nm below surface, the microstructure of multilayer is similar to that of the as-deposited films.

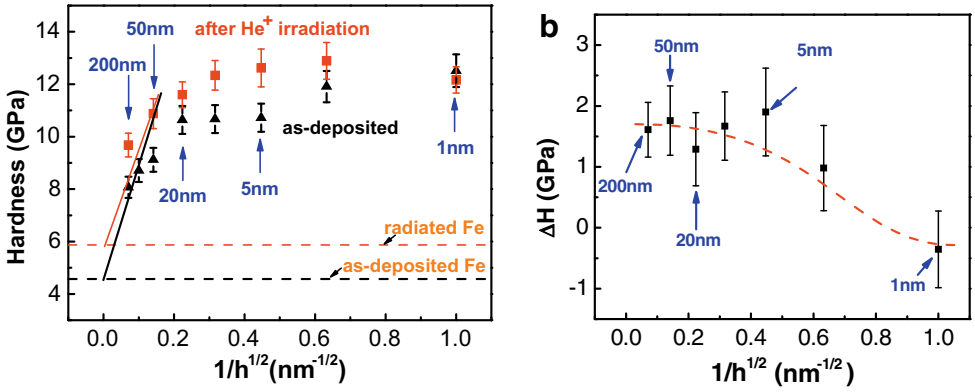

Fig. 6. (a) Comparison of hardness as a function of $h^{-1/2}$ plots for as-deposited and ion irradiated Fe/W multilayer films. The hardnesses of multilayers with layer thickness of greater than 50 nm are fitted by using solid lines, indicating that the Hall–Petch dislocation pile-up model can describe strengthening in this regime. The hardnesses of as-deposited and ion irradiated single layer Fe film are also shown as two dash lines. (b) The plot of hardness enhancement vs. individual layer thickness shows that hardnesses increase by about 1.5 GPa for $h \geqslant 5$ nm specimens. When h is $\leqslant 2.5$ nm, the hardness only increases slightly or barely changes.

4. Discussion

4.1. Microstructural evolutions

We will first examine radiation induced microstructure changes. XRD studies show that peak intensity of Fe (1 1 0) and W (1 1 0) decreases after He ion irradiation, and peak positions shift to lower angle. Reduction of peak intensity is an indication of disordering of crystal lattices due to radiation induced point defects, and peak broadening is often associated with microstrain due to entrapment of interstitials. Decrease of peak angle is an indication of enlargement of lattice spacing in a direction normal to inter-

faces. Radiation induced lattice expansion was also confirmed by SAD patterns in TEM studies. Lattice expansion in Fe and W is likely to be a result of interstitials, including He interstitials and Fe and W self interstitials, and interstitial loops when loop diameter is on the order of nanometer length scale. Also intermixing of Fe and W due to radiation is likely to occur along layer interfaces, as Fe and W are miscible. Intermixing could lead to the formation of Fe–W solid solutions along interfaces and thus lead to distortion of lattices. XTEM studies show that the average bubble diameter in Fe is slightly larger than that in W. Based on the relationship: $p = 2\gamma/r$, where γ is the surface energy, and r is the radius of He bubble, the critical He concentration to nucleate He bubbles is proportional to γ, which typically scales proportionally with shear modulus [6]. Hence the difference in He bubble diameter may originate from the difference in shear modulus and surface energy between Fe and W [16]. Furthermore we noticed that He bubbles tend to have larger diameter with ellipsoidal shape along interface. This phenomenon has been observed in other systems [17]. A larger diameter (radius) of He bubbles along interface indicates that internal pressure and surrounding equilibrium pressure of He is lower.

4.2. Possible hardening mechanisms

We will first interpret radiation hardening, ~1.8 Gpa, in Fe/W 50 nm multilayers and then comment on size (layer thickness) dependent radiation hardening.

Two major mechanisms have been proposed [18,19] to explain radiation hardening: the dispersed barrier hardening, where radiation induced defects (such as vacancy or interstitial clusters) act as barriers to the movement of dislocations, and the source hardening, the increase in stress required to start a dislocation moving on its glide plane. Since the contribution of source hardening is relatively small, we will focus on dispersed barrier hardening model, which describes the flow stress required to sustain plastic deformation. In the case of Fe/W multilayers, radiation induced hardness variations are likely to originate from He bubbles, interstitial loops, He interstitials, and the microstructural evolution of layer interface (such as intermixing).

4.2.1. He bubbles

In order to estimate the hardness enhancement by He bubbles, it is necessary to obtain He bubble density. Assuming the thickness of TEM sample is around 100 nm, from XTEM images captured at different depths, the density of He bubbles can be estimated and results are shown in Fig. 7. The cubic and triangle dots in Fig. 7 stand for He bubble density in Fe/W 50 nm and Fe/W 1 nm multilayers, respectively, and the dash line and the dash–dot line are used as visual guides. The evolution of bubble density with depth is somewhat consistent with the SRIM prediction of He concentration vs. depth. The average He bubble concentration, N, is similar in both cases, namely $1.1 \times 10^{24}/m^3$ and $0.9 \times 10^{24}/m^3$ in Fe/W 50 nm and Fe/W 1 nm multilayers, respectively.

We now attempt to estimate He bubble induced hardening in Fe/W 50 nm multilayers. For weak obstacles, such as He bubbles [7,8,20,21], a hardening relationship developed by Friedel–Kroupa–Hirsch (FKH) can be used to describe the dependence of radiation hardening on He bubbles [22–24]:

$$\Delta\sigma = \frac{1}{8} M\mu b d N^{2/3}, \tag{2}$$

where M is Taylor factor, 3.05 for BCC metal, μ is the shear modulus, b is the Burgers vector. The increase in yield stress from FKH model is calculated to be ~0.13 GPa, corresponding to a hardness increase of 0.4 GPa. Thus radiation hardening due to He bubbles is very small comparing to experimental values.

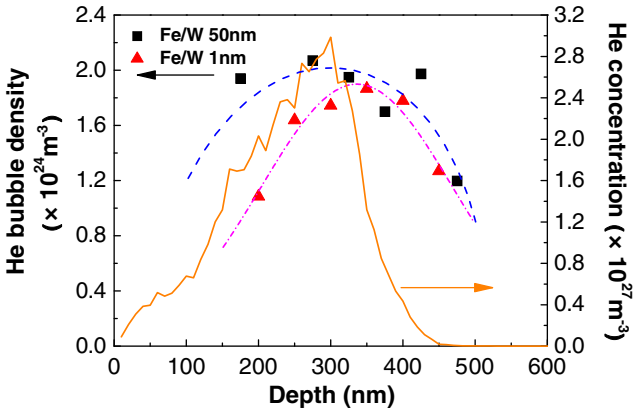

Fig. 7. Depth dependent He bubble density in irradiated Fe/W 1 nm and Fe/W 50 nm multilayer films. Superimposed is the He concentration profile for Fe/W 50 nm multilayers simulated from SRIM code.

4.2.2. Dislocation loops

Based on a dispersed barrier hardening model [25], the increase in yield stress $\Delta\sigma_y$ is equated to the increase in applied stress required to move a dislocation through a field of obstacles:

$$\Delta\sigma_y = M\alpha\mu b/l = M\alpha\mu b\sqrt{Nd}, \tag{3}$$

where α is the barrier strength, and l is the average spacing between obstacles, and can be estimated as $1/\sqrt{Nd}$, where N and d is the average loop density and loop diameter, respectively. Considering the typical barrier strength of dislocation loops, α is taken as 0.45 [26,27]. An experimental determination of loop density is not yet available due to the difficulty of imaging dislocation loops in nanocrystalline metallic multilayers. Under the assumption that radiation hardening is originated primarily from dislocation loops and considering partial contribution from He bubbles, our analysis yields a dislocation loop density of $2 \times 10^{22}\ m^{-3}$ when the loop diameter is ~5 nm. Zinkle and Singh investigated the microstructure of neutron irradiated Fe, and found the defect cluster density and cluster loop diameter increase with increasing dose [28]. When the dose increased from 0.0001 to 0.79 dpa, the loop density increased from 1×10^{21} to $6 \times 10^{22}\ m^{-3}$ and the loop diameter increased from 1 nm to 4 nm. In He ion irradiated Fe/W multilayers, the peak damage is ~6 dpa, and the estimated loop density is comparable to that observed in neutron irradiated Fe.

4.2.3. He interstitials

Although some He atoms have been combined with vacancy to form He bubbles in the multilayer films, there are still a large number of isolated He atoms or He clusters in the system. Atomic simulations [29] show that at low temperature, He interstitials in the vicinity of a dislocation can easily migrate to the dislocation core, and thus resist the glide of dislocations. The binding energy of He to dislocation line is around 2 eV [29]. From Fig. 7, the average He concentration is calculated to be around $1 \times 10^{27}\ m^{-3}$, much higher than He atoms reside within He bubbles. Previous studies have shown that high concentration of He interstitials will lead to hardening especially when He concentration approaches a critical value, ~1 at.% [6,7,9], or a critical dose of >1 dpa. However quantitative analysis of He interstitial induced hardening is difficult given the difficulty of determining He concentration within lattices.

Given the estimation of small radiation hardening from He bubbles and the difficulty in measuring dislocation loop density, the interpretation of radiation hardening mechanisms in Fe/W 50 nm multilayers is complicated. Nonetheless, radiation hardening may

originate mainly from dislocation loops and partially from He bubbles and interstitials.

Hardness of irradiated Fe/W 1 nm multilayers barely changes, very different from radiation induced hardening in films with $h \geqslant 5$ nm. XTEM studies show that in peak damage zone the layered structure cannot be resolved in through-focus images of Fe/W 1 nm multilayer presumably due to radiation induced intermixing. It is known that peak strength of as-deposited nanolayer films are determined by interface barrier strength to the transmission of single dislocations [30]. The loss of layer interface may degrade the hardness of multilayers. Such an effect may counteract radiation induced hardening. Finally a noticeable reduction of Hall–Petch slope after radiation indicates a less dependence of hardening on layer thickness as a result of abundance of radiation induced defects in multilayers. Details will be discussed elsewhere.

5. Conclusions

The present studies reveal that after He ion irradiation to a fluence of $6 \times 10^{16}/\text{cm}^2$, a large number of He bubbles were observed in both Fe and W, and peak He bubble density occurs at a similar location compared to the peak lattice distortion of Fe (110) and W (110). Radiation induces hardening in multilayers when $h \geqslant 5$ nm specimens. At such length scales, analyses indicate that radiation induced hardening may originate mainly from dislocation loops and only partially from He bubbles. Hardness barely changes in irradiated Fe/W 1 nm specimens as a result of diminishing discreteness of layer interfaces due to intermixing.

Acknowledgements

This research is funded by DOE-NERI, Office of Nuclear Energy, Science and Technology, AFCI program, under Grant No. DE-FC07-05ID14657. A. Misra et al. from Los Alamos National Laboratory (LANL) acknowledge support by the US DOE, Office of Science, Office of Basic Energy Sciences. X. Zhang acknowledges support by DOE-Center for Integrated Nanotechnologies (CINT) for the access of their facilities. Authors also acknowledge discussions with Dr John G. Swadener at Los Alamos National Laboratory and Dr Z.P. Luo, from Microscopy and Imaging Center at Texas A&M University.

References

[1] F. Carsughi, H. Ullmaier, H. Trinkaus, W. Kesternich, V. Zell, J. Nucl. Mater. 212 (1) (1994) 336.
[2] H. Trinkaus, W.G. Wolfer, J. Nucl. Mater. 122 (1984) 522.
[3] [a] H. Trinkaus, Radiat. Eff. 78 (1983) 189;
[b] A.W. Thompson, Mater. Sci. Eng. 21 (1975) 41.
[4] H. Trinkaus, H. Ullmaier, J. Nucl. Mater. 212 (1) (1994) 303.
[5] E.V. Kornelsen, A.A. Van Gorkum, J. Nucl. Mater. 92 (1980) 79.
[6] H. Trinkaus, B.N. Singh, J. Nucl. Mater. 323 (2003) 229.
[7] H. Trinkaus, J. Nucl. Mater. 38 (2003) 234.
[8] G.E. Lucas, J. Nucl. Mater. 206 (1993) 287.
[9] J.D. Hunn, E.H. Lee, T.S. Byun, L.K. Mansur, J. Nucl. Mater. 282 (2000) 131.
[10] X. Zhang, N. Li, O. Anderoglu, H. Wang, J.G. Swadener, T. Hochbauer, A. Misra, R.G. Hoagland, Nucl. Instrum. Meth. Phys. Res. B 261 (2007) 1129.
[11] T. Hochbauer, A. Misra, K. Hattar, R.G. Hoagland, J. Appl. Phys. 98 (2005) 123516.
[12] A. Misra, M.J. Demkowicz, X. Zhang, R.G. Hoagland, JOM 59 (2007) 62.
[13] H.L. Heinisch, F. Gao, R.J. Kurtz, J. Nucl. Mater. 329–333 (2004) 924.
[14] R. Popescu, H.L. Meyerheim, D. Sander, J. Kirschner, Phys. Rev. B 68 (2003) 155421.
[15] J.F. Ziegler et al., The Stopping and Range of Ions in Solids, 1985.
[16] J.P. Hirth, J. Lothe, Theory of Dislocations, second ed., Krieger Publishing Company, 1982.
[17] P.A. Thorsen, J.B. Bilde-Sorensen, B.N. Singh, Scr. Mater. 51 (2004) 557.
[18] D. Rodney, G. Martin, Phys. Rev. Lett. 82 (1999) 3272.
[19] Gary S. Was, Fundamentals of Radiation Materials Science, Springer, Berlin, Heidelberg, New York, 2007.
[20] G.R. Odette, D. Frey, J. Nucl. Mater. 85&86 (1979) 817.
[21] A.L. Bemment, in: Proceedings of the Second International Conference on the Strength of Metals and Alloys 2, ASM, 1970, p. 623.
[22] S.J. Zinkle, Y. Matsukawa, J. Nucl. Mater. 329–333 (2004) 88.
[23] Friedel, Dislocations, Pergamon, New York, 1964.
[24] F. Kroupa, P.B. Hirsch, Discuss. Faraday Soc. 38 (1964) 49.
[25] A.K. Seeger, in: Second UN Conference on Peaceful Uses of Atomic Energy, vol. 6, United Nations, New York, 1958, p. 250.
[26] M. Grossbeck, P. Maziasz, A. Rowcliffe, J. Nucl. Mater. 191–194 (1992) 808.
[27] F. Garner, M. Hamilton, N. Panayotou, G. Johnson, J. Nucl. Mater. 103&104 (1981) 803.
[28] S.J. Zinkle, B.N. Singh, J. Nucl. Mater. 351 (2006) 269.
[29] H.L. Heinisch, F. Gao, R.J. Kurtz, E.A. Le, J. Nucl. Mater. 351 (2006) 141.
[30] R.G. Hoagland, J.P. Hirth, A. Misra, Philos. Mag. 86 (2006) 3537.